Real-Time Surveillance of LEO and MEO
with Small Optical Telescopes

Peter Zimmer
J. T. McGraw and Associates, LLC

John T. McGraw
J. T. McGraw and Associates, LLC
University of New Mexico

Mark R. Ackermann
J. T. McGraw and Associates, LLC

ABSTRACT

J.T. McGraw and Associates, LLC operates two proof-of-concept wide-field imaging systems to test novel techniques for uncued surveillance of LEO/MEO/GEO and, in collaboration with the University of New Mexico (UNM), uses a third small telescope for rapidly queued same-orbit follow-up observations. Using our GPU-accelerated detection scheme, the proof-of-concept systems operating at sites near and within Albuquerque, NM, have detected objects fainter than V=13 at greater than 6 sigma significance. This detection approximately corresponds to a 16 cm object with albedo of 0.12 at 1000 km altitude. Dozens of objects are measured during each operational twilight period, many of which have no corresponding catalog object.

The two proof-of-concept systems, separated by ~30km, work together by taking simultaneous images of the same orbital volume to constrain the orbits of detected objects using parallax measurements. These detections are followed-up by imaging photometric observations taken at UNM to confirm and further constrain the initial orbit determination and independently assess the objects and verify the quality of the derived orbits. This work continues to demonstrate that scalable optical systems designed for real-time detection of fast moving objects, which can be then handed off to other instruments capable of tracking and characterizing them, can provide valuable real-time surveillance data at LEO and beyond, which substantively informs the SSA process.

1. Introduction and Background

Small optical telescopes, deployed strategically across the globe, hold the potential to contribute significant and complementary capabilities to space situational awareness (SSA), beyond their current roles in monitoring and characterizing objects in and near the geosynchronous regime. The work demonstrated here shows proof-of-concept solutions to several of the challenges to making small optical telescopes viable for uncued surveillance of LEO and MEO. We also show how some of these techniques can be applied to imagery taken with larger telescopes to find faint objects that are often missed by standard astronomical image processing techniques.

For objects that have well-understood motions, many existing observational resources can be brought to bear to study it. In the case we are interested in, the objects in question are either not known, were lost or have maneuvered away from their previously known motions. Because we are focused on uncued surveillance, there are choices that can be made about how to optimize the design and operate the telescope system. If some foreknowledge of a target's position and rate are available, the best measurement signal-to-noise ratio is obtained by tracking that rate and acquiring images where the signal integrates within a few resolution elements. Incomplete knowledge of rates causes moving objects to leave streaks in images when the exposure time is long compared to the time it takes for the object to move to an independent resolution element. This effect is often referred to as trailing loss, because the signal-to-noise per resolution element decreases proportionally to the number of resolution elements that are illuminated. The object only dwells in a given resolution element for a small fraction of the exposure time but the background is contributing noise for the entire exposure. Thus, a bright object that might be an easy detection while tracked becomes a faint streak that is far more challenging to detect and measure.

For uncued surveillance, while rates are not known ahead of time, upper and lower limits can be placed based on orbital regimes of interest and physically admissible regions, so one must either take images so fast that the object appears fixed, or find ways of detecting and measuring streaks. Under ideal circumstances, where detector noise and data processing are not obstacles, the fast image acquisition would be clearly superior. Optimal signal-to-noise would be achieved in each image and techniques would search through stacks of images for things that move. In general, rapidly reading out a detector leads to dramatically increased detector noise, thereby obviating the gain in signal-to-noise. Moreover the increased data volume generated can also become unmanageable – requiring significant computing resources for each small telescope defeats one of the key strengths of using optical detection in the first place – its low cost. Fast-framing is the approach used by systems such as GEODSS [1], but in this case it is for relatively slow moving objects at GEO and quickly loses efficacy for faster moving objects. Thus, barring some significant developments in detector, data storage and computational technology, optical SSA for fast moving objects necessitates streak detection.

In Section 2, we detail the telescope systems that JTMA has fielded to test and demonstrate real time optical detection and follow-up. These systems monitor a small volume of LEO and MEO above their respective observatories and image the objects that cross the field of view – we summarized previously reported results in Section 3. JTMA personnel developed software solutions to the problem of streak detection that scale well to consumer grade computing systems by use of GPUs and we demonstrate some selected results in Sections 4 and 5. In Section 6, we apply these same software approaches to an existing GEO debris survey data set from one of the 6.5m Magellan telescopes.

2. Optical Detection System Description

We reported on the design of these systems previously [2] and we briefly review them here. The systems are based upon commercially available components which provide the most cost-effective solution for a real demonstration and test bed for our techniques. Commercially available detectors place the most constraining limits on the design space, principally because they have been designed for some other purpose than wide field astronomical observations. Budgetary constraints effectively eliminated backside illuminated CCDs, which are desirable for their high quantum efficiency, though they do require a mechanical shutter and the readout time overheads are often of the order 100% for one second cadence images. Our need for rapid observing cadence with minimal dead time drove us to use 35mm format interline CCDs that are commercially available in cameras from several vendors, because they can be read out while the next exposure is accumulating, eliminating readout overhead. Non-interline, front illuminated sensors were eliminated because the readout time overhead reduced the allowable exposure times, despite the availability of physically larger sensors. CMOS sensors hold a great deal of promise for the future, but at present they are both expensive and physically too small to create a large field of view (FOV) for telescopes with appreciably large apertures.

The systems presently in operation are based around a 14" Celestron Schmidt-Cassegrain optical tube with a HyperStar f/1.9 prime-focus corrector. Combined with an ON Semiconductor (formerly TrueSense (formerly Kodak)) KAF-16070 4864 x 3232 sensor with 7.4 micron pixels, this gives a 3° x 2° field of view with 2.23 arcsecond pixels, albeit with significant vignetting in the corners of the field (illumination in the corners is roughly 50% that of the field center). This vignetting is caused primarily by the aperture of the corrector plate at the entrance aperture of the Schmidt-Cassegrain design, which was never intended to operate over such a large field. The CCD is integrated into Finger Lakes Instruments Microline cameras, which were chosen because they allowed a rapid dual amplifier read rate of 12MHz each, resulting in a 1Hz frame rate (principally limited by the USB2.0 bus) in a compact housing with integrated thermoelectric cooling, reducing dark current noise to a largely negligible level. Because these cameras are operating at prime focus, the form factor is critical to preclude adding to the system obscuration, and the Microline camera adds only a small fraction compared to the Hyperstar corrector housing. The net result is an instrumental etendue of almost 0.5 m^2deg^2 for a 6 square degree FOV that can read out at 1 Hz with 11e- of read noise, essentially zero dead time (< 5 μs) between exposures, with parts available off-the-shelf for around $20,000 for the telescope, corrector and camera.

We have deployed two of these systems in the Albuquerque metropolitan area, as shown in Figures 1 and 2. Siting telescopes this close to a major population center is not ideal from a sky brightness standpoint and incurs a cost in detectivity, especially for the system within Albuquerque city limits, but it provides easily accessible systems for development and testing. The added noise from night sky background illumination is easily quantified and we can readily extrapolate the performance that would be expected from a dark sky site. Given the relatively small apertures involved and the rapid image cadence, a truly dark astronomical site (West Texas, Hawaii, Chile, etc.) is not crucial for LEO observations. For GEO observations metropolitan locations definitely compromise sensitivity, because the

objects are inherently fainter and their apparent rates are slow enough to allow longer exposure times and therefore higher accumulated background. Still, they are quite useful for testing purposes even for GEO observations.

Each telescope and camera system is installed on a Paramount MX German Equatorial mount allowing precision pointing and very reliable operation. These are attached to Parallax Instruments portable piers and installed in 7 foot diameter Astrohaven domes. The deployed systems in their domes are shown in Figure 2. Altogether - optical systems, mounts, domes and computers - the total cost per system is approximately $50,000, and the entire system can be deployed by a small team in about two hours, crate-to-sky, so mobility is an option.

We have also upgraded the mount and dome of a 312mm f/5 telescope at the University of New Mexico Campus Observatory (UNMCO) so that it can rapidly and autonomously follow-up on detections made with the wide-field detection systems. This system results in a 1.0 x 0.6 degree field of view, but unlike the detection systems, which are unfiltered, this system can take either unfiltered or canonical BVRI filtered images.

Figure 1. JTMA's Proof-of-Concept LEO SSA Optical Systems are separated by 27 km enabling them to simultaneously observe the same volume of LEO and obtain range estimates based on parallax for objects detected with both systems.

Figure 2. The northern JTMA Proof-of-Concept LEO SSA Optical Systems shown enclosed and opened to the sky awaiting twilight. The optical systems are 14" Celestron Schmidt-Cassegrain telescopes with Hyperstar prime focus wide field correctors installed. A FLI ML-16070 interline CCD provides a 3° x 2° field of view with 2.25" pixels and can be read out at 1 Hz with no deadtime between frames. The systems are enclosed in 7ft Astrohaven clamshell domes.

3. **Summary of Previously Reported Results**

In order to offer some insight into the performance into the capabilities of these detection systems, we refer to our previously reported results [3, 4 and 5] and briefly summarized here:

- Objects in LEO are bright by astronomical standards
  - A 10cm object at 1000km ~12th magnitude (A=1) to 14th magnitude (A=0.12)
  - A golf ball (4.2cm) at 1000km range with a 90% albedo is ~14th magnitude
  - Even under bright skies, a 16th mag. star is bright enough to detect in 1s with a 300mm telescope

- Objects in LEO have a high apparent angular velocity:
  - ~0.2 deg/s at 2000km, 0.4 deg/s at 1000km, and up to ~1.5 deg/s at 300km, observed near zenith.
  - Light from LEO objects is therefore trailed over many pixels, each of which contributes read noise and sky background noise – so-called trailing losses.
  - The resulting loss in per-pixel signal-to-noise ratio scales as the number of pixels in the streak, which can be hundreds to thousands of pixels long.

- Signal-to-noise (S/N) in the whole LEO streak is more significant than the per-pixel S/N by approximately the square root of the streak length
  - If you can find the streak it in the first place.
  - The low per-pixel S/N is most often ignored as part of the background by traditional source detection techniques because the per-detection-kernel S/N does not cross a statistical significance threshold.

- Rapid cadence (~1s) imaging with zero deadtime of wide instantaneous fields of view (FOV >> 1 square degree) can catch LEO objects as they streak through the field
  - Exposure time tailored so that a 1 deg/s object will cover half of the FOV.
  - Zero deadtime for maximum efficiency and no lost objects between exposures.
  - Optimize for existing hardware, read noise and feasibility of real time detection.
  - Detector deadtime from shuttering and readout of typical full-frame detectors has the same effect as an overall lower quantum efficiency.

- Astrometric and Photometric Performance of Proof-of-Concept Detection Systems
  - Each 2˚ x 3˚ FOV typically contains 1000+ UCAC4 astrometric standard stars
  - Typical astrometric residual w.r.t. UCAC4: 0.25-0.35 arcseconds rms
  - Limiting magnitude (6 sigma) for stars: ~15 for bright conditions, ~16 in dark skies in one second

- Example of Streak Detection Performance at LEO
  - 11.6 magnitude object moving 2,720 arcseconds per second detected at 8.6 sigma
  - Implied circular orbit altitude: 600km
  - Implied size: 20cm – assuming diffuse sphere with 0.12 albedo

- Example of Streak Detection Performance at MEO
  - Highly variable object, magnitude fluctuated dramatically between 11.3 & 13.2 over 15 seconds of dwell time in FOV
  - Apparent angular rate: 460 arcseconds per second.
  - Implied altitude: 4,435 km with inclination of 105˚
  - Intensity changed by factor of 4 in 2 seconds, and even faster within exposure time

- Streak Detection Performance near GEO
  - Magnitude 15.7 super-GEO object detected at 7 sigma in 5 second exposure

- Parallax Range Determination
  - 27km separation of telescopes allows range determination
  - Apparent parallax for object at 1000km is 1.5 degrees
  - 1 pixel (2.23") rms error in position in this case is ~750m range error
  - Parallax can even be useful at GEO ranges

- Current LEO Mode Execution Time Performance
  - 0.9s per 2x2 binned image, of which preprocessing takes 0.4s and detection code 0.5s

o Star mask and noise model computed once per minute or as needed, taking up to 8 seconds
o Maximum time from detection to TLE generation: 4 seconds.

4. Simple Streak Orbit Determination

One of the driving goals of JTMA's optical detection system is to be able to be able to detect a LEO object and trigger immediate, same-pass follow-up observations with other nearby (and distant) telescopes. Even with the large fields of view covered by the detection systems, low altitude objects are only observed for a few seconds altogether. A new detection needs to be passed off so that the object's orbit can be further refined, reducing the chance that it is lost and enabling even more follow-up observations with larger telescopes and more diverse instruments.

Fortunately, a single streak measurement incorporates more information than just a single pair of angles only RA & Dec coordinates. RA and Dec rates are also embedded in the streak length and orientation. Those four parameters are enough to constrain two possibilities of an approximate circular orbit, where the direction of travel along the streak is not known from a single observation. That directional degeneracy is broken with a second image, even if in that image the streak is truncated by the edge of the detector. Bear in mind that this is not meant to be a rigorous initial orbit determination at this point, but simply a way to be able to task immediate follow-up resources, in less than 30 seconds at present and ultimately in less than 10 seconds. On this timescale, having the orbital plane and current apparent rate is good enough to constrain the motion on these short timescales. This approach expands on the work of Michael Earl [6], which assumes near-zenith pointing, to a more general solution with arbitrary pointing.

From a single site, a detected streak yields two endpoints with measured angular positions defining two lines of sight, **A** and **B**, which must be corrected for the effects of aberration and light travel delay, referenced to ICRS coordinates. Combined with the known inertial location of the observatory site at the beginning and end of exposure, call them X_1 and X_2, which are different because the Earth has rotated during the exposure, two possible sets of two lines of sight are defined, depending on whether the object was moving from **A** to **B** or **B** to **A** – with only one observation the direction of travel along the streak is unknown. Each of those two line of sight combinations can yield a simple orbit estimate. Consider the first combination, $X_1 \rightarrow A$ and $X_2 \rightarrow B$. There is a single parameter family of circular geocentric trajectories that go through both of these lines of sight, each of which has a velocity set by the crossing time between the lines of sight, which is the image exposure duration. Only one of these circular trajectories corresponds to an orbit with a physically correct circular orbit velocity for its radius. The degeneracy between directions of travel can be broken with the subsequent image. The two possible solution are not, in general, time-symmetric, but usually have significantly different orbital parameters because of the motion of the ground station between the beginning and end of the exposure.

We have successfully used this technique to determine the trajectory of several objects that were initially detected with our southern observation site, which then handed off TLEs to the UNMCO telescope. The UNMCO system then moved and obtained follow-up observations in under one minute, continuing to move and image until the objects moved below the horizon. As expected, the assumption of a circular orbit leads to systematic offsets when the object is in an orbit that deviates significantly from circularity. However, the intent is to use this estimate in a very short time window after the detection, during which the deviations from the circular approximation are small compared to the FOV of the telescope making the follow-up observations. Moreover, the determination of the orbit plane is quite robust, so that uncertainties in the apparent position for the follow-up telescope are mostly in the along-track direction. The detailed results are preparation.

5. Some Selected Detections and Results

During any given twilight LEO-mode operation session, there are typically between 300 and 600 images that contain detected streaks out of 5000-7000 images obtained. Some of these objects appear in only one image, while some bright, slow objects can appear in a hundred or more. We include two example object detections as demonstrations of objects that can be detected with these systems.

Figures 3-5 show the fastest moving object we have definitively detected so far. It is not likely to have been a meteor, because it is detected in two frames whereas meteors will generally have much higher apparent rates – meteor re-entry occurs lower in the atmosphere and the meteor particles will typically have a much higher velocity, both of which result in typical angular rates much higher than this. This particular object gets dramatically brighter as is moves across the field in excess of 1.1 degrees per second and detected at 13.2σ. The starting point of the streak on the left hand side of Figure 3 is not distinct due to the increasing brightness and the point marked is the statistically most likely endpoint as determined by our processing pipeline. There is no indication of it in the preceding image, nor is it detected

with the second telescope, but given the altitude implied by the rate, this is not surprising as their fields were configured to overlap at a higher altitude. The simple orbit determination used with these endpoints gives an altitude of 417.2 km with inclination of 143.08° and given that range, this corresponds to a sphere of approximate diameter 13 cm, assuming a diffuse reflector with albedo 0.12. At this altitude though, the object is likely to be passing through the penumbra because the Earth's shadow is close to this region and this may explain the change in apparent brightness. As such, this size estimate should be treated as a lower limit. The altitude estimate also is uncertain due to the lack of definition in the initial streak point. However, it can't be very much longer, or its velocity would correspond to a much lower altitude that would be in shadow. There are not any likely counterparts to this object in Space-Track [7].

The same subfield of the subsequent image is shown in Figure 4. Unfortunately this portion is clipped by the edge of the field, but even with only 60% of the streak length available, this section is twice as bright as in Figure 3, which given the range estimate above, the size of this object is probably 40%+ larger than estimated from the previous image, or approximately 20 cm, assuming that its orientation didn't change. The combination of these along with the detection significance shows that our detection limit for an object at this altitude is below 10 cm.
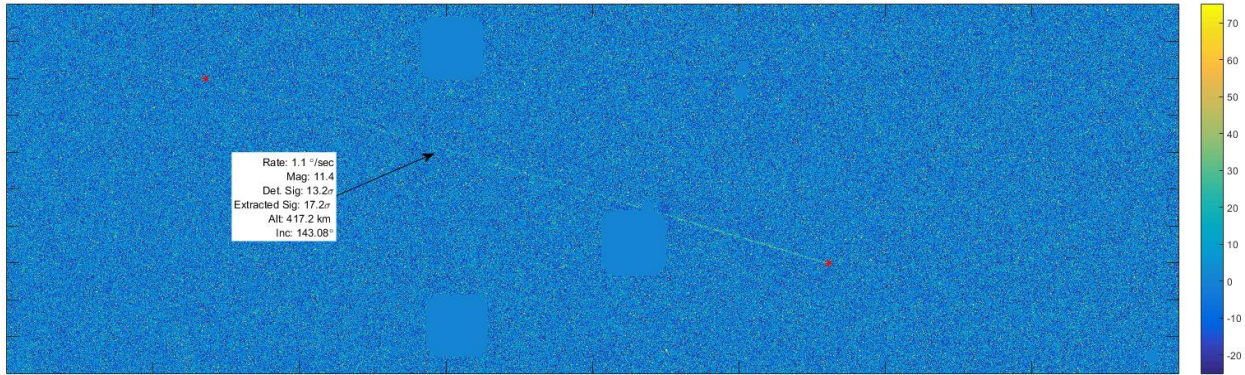

Figure 3. 0.6 x 2.0 degree subfield showing the initial detection of fast moving object, detected at 13.2σ with a rate of 1.1°/sec and magnitude of 11.4. This corresponds to an object of ~13 cm diameter (diffuse sphere, A=0.12) in a circular orbit of altitude 417.2 km.
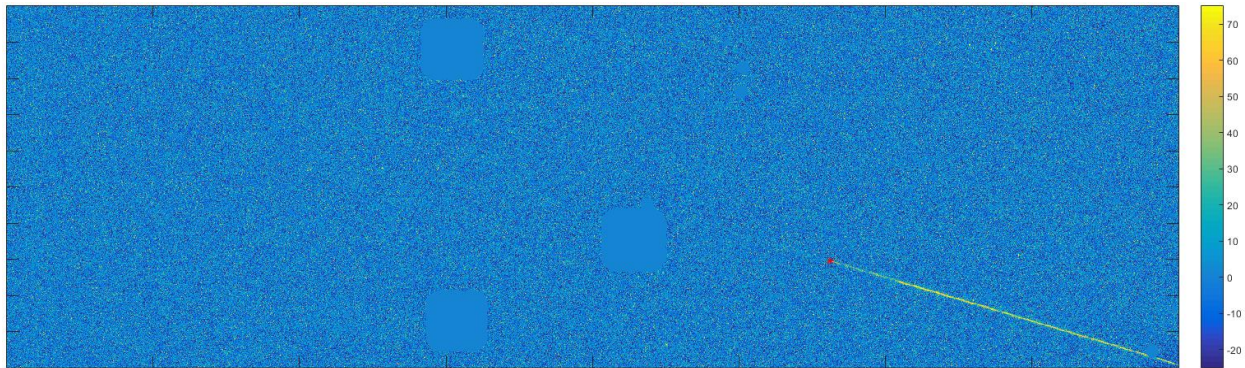

Figure 4. Same object in subsequent image. This object gets dramatically brighter within this field and overall, and even though the streak is cut off by the edge of the detector at the bottom, its integrated signal is 0.7 magnitudes brighter than that in Figure 5.

Figure 5 shows the light curve of this object as extracted in a three pixel wide aperture along the streak. The orange line corresponds to the frame in Figure 3, the blue line to Figure 4. This also shows that while your eye may see an extension of the streak in Figure 4 to the left of the red dot, this feature is not real and is not present in the full image.
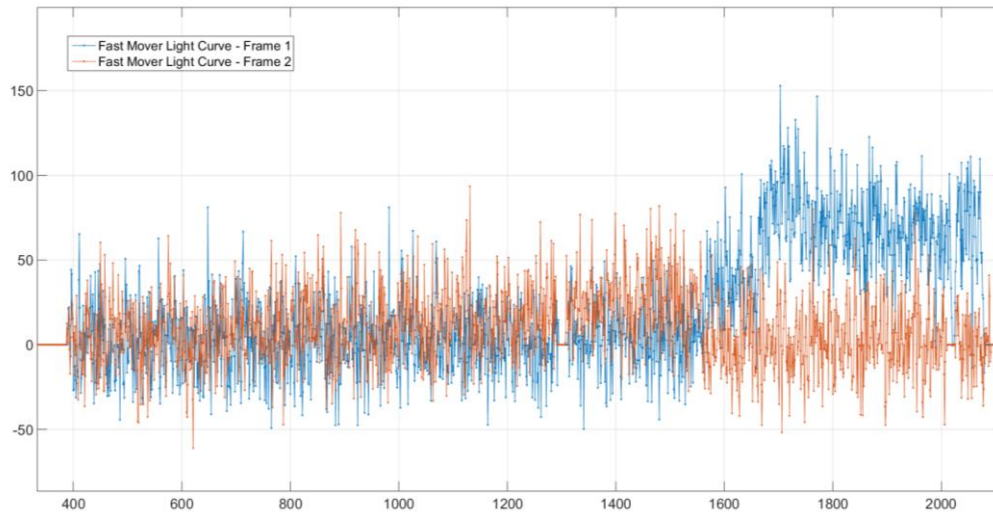
Figure 5. Extracted light curves from the detections shown in Figure 5 (orange) and Figure 6 (blue). In this representation, the object moved left to right and the most likely starting point is near 700 on the x-axis, where each point is the equivalent of a 2x2 binned pixel on the detector, 4.45 arcseconds wide and the vertical axis is in detected electrons.

The second example is an object moving much more slowly and modulating rapidly in intensity. This object is shown in a series of 0.12˚ x 0.12˚ sub-images that span 42 consecutive 1s exposures displayed in Figure 6. This object was on the edge of detectability for LEO-mode observations which is optimized for longer streaks – and clearly this is well above the LEO regime – only three of these images resulted in automated detections, with the rest extracted on the basis of those detections. This object has an average magnitude of 12.9 in these three frames and is detected at maximum 6.9σ significance. After performing the simple orbit determination, it was clear that this object is in the Space-Track catalog, EXPLORER 38 DEB (ID 3848) – presumably some piece of the Radio Astronomy Explorer A spacecraft [8].

While we cannot find documentation on what this piece of debris is, it is from a well-known mission. The debris has a measured radar cross-section of 0.69^* m^2. This allows us to run some sanity checks on our detection processes to see if our detection limits are as expected, by using this cross section to estimate an equivalent spherical diameter [9] of roughly 90 cm. The comparison point that we typically use for our LEO detection techniques is the equivalent diameter object detectable in a 1000 km altitude circular orbit. Basic radiometric estimates [10] predict that a Lambertian sphere of diameter 10 cm and 12% albedo will have an approximate magnitude of 14 in V band under terminator illumination conditions (Φ=90˚). In the same way as for the radar cross section to physical size estimates, there are numerous instances of 'all else being equal' but this gives some insight into brightness vs. size relationships which are otherwise complex.

Apparent optical intensity in this diffuse scattering model scales proportionally to the characteristic size squared and inversely proportional to distance squared, so these two can be traded off directly. Thus a 90 cm object at 5,850 km will have a similar intensity as a 15.4 cm diameter object at 1000 km with the same reflectivity. A 12% diffuse sphere would be magnitude 13.1, so this object appears about 20% brighter than this estimate. Figure 7 shows the extracted light curve of these measurements, which demonstrates significant glinting (2+ mag.), so the diffuse model is assuredly unrealistic. As a sanity check and performance demonstration however, this succeeds.

---

* Space-Track recently stopped publishing the numerical values for radar cross section, but they still exist in several places for older objects. This value was taken from http://www.n2yo.com/satellite/?s=3848#results on August 5, 2015.
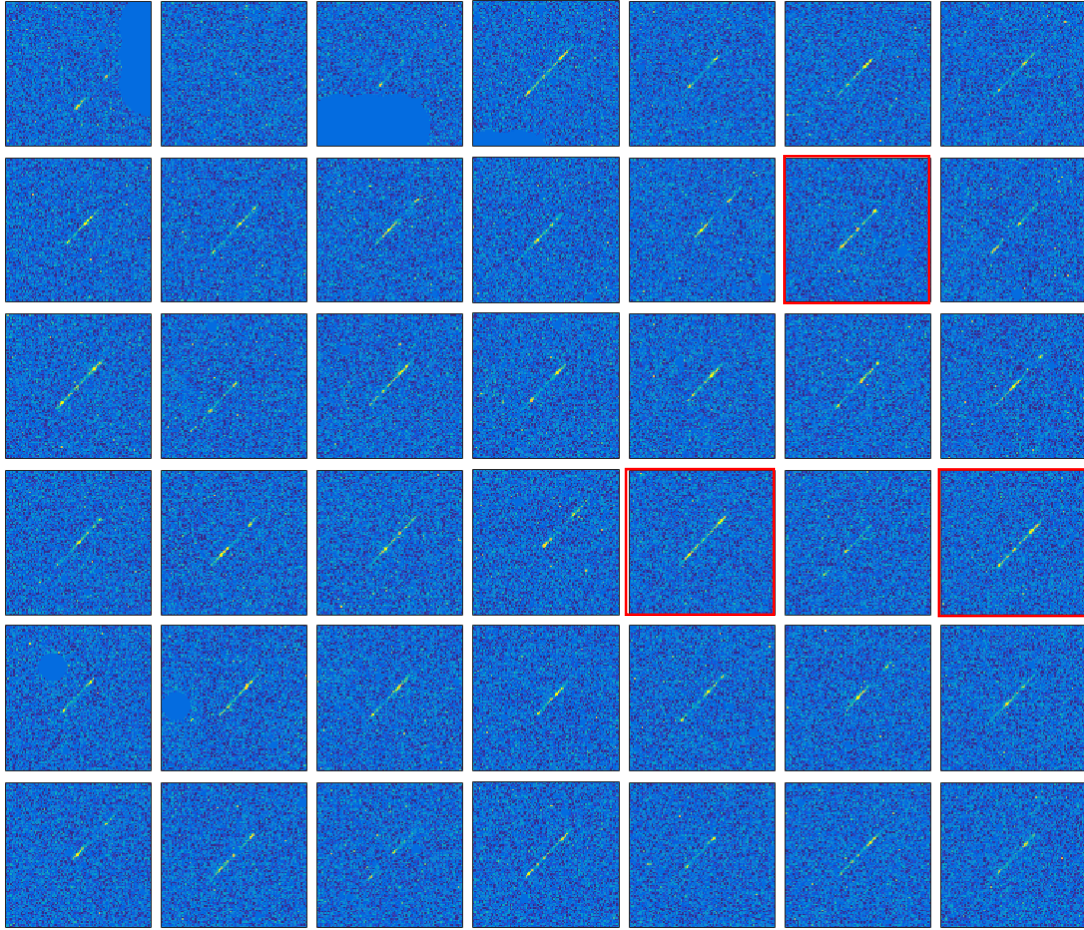
Figure 6. Sequence of sub-images showing EXPLORER 38 DEB (NORAD ID 03848), a faint, slow moving object in MEO that shows rapidly modulating intensity. Each box is taken from a one second exposure. The first exposure is in the upper left, with subsequent exposures left-to-right, then top-down. The red boxes indicate the frames where EXPLORER 38 DEB was detected by the LEO-mode detection system. Color map scaled to show -1σ to +5σ of the image noise. In each sub-frame, the object is moving up and to the right.
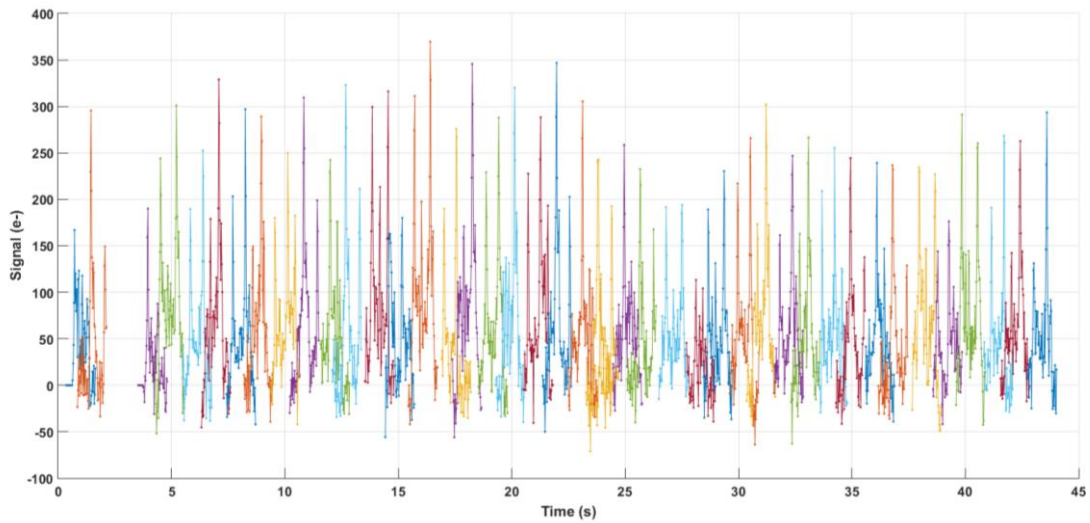

Figure 7. Extracted light curve of Explorer 38 Debris as measured by the LEO mode detection system. Strong, periodic glints are obvious, modulating the measured intensity by a factor of 6 or more (2+ magnitudes).

6. Application of Streak Detection to Existing Data Set

For the purpose of testing and evaluating various faint object detection techniques, Pat Seitzer of the University of Michigan shared 9 images with JTMA from a set of untracked Magellan images obtained for the GEO Debris Survey on the Magellan 6.5m Baade telescope using the IMACS f/2 camera [11]. Each image is a 5 second r-band exposure taken 36 seconds apart. The resulting 4300 x 4300 pixel image is a 2x2 binned composite from the 8 device CCD mosaic focal plane registered to a common pixel grid with a net image scale is 0.4" per pixel.

Photometric calibration was obtained on the same night [12] and allows us to cast these results into r-band magnitudes and estimate sizes based on equivalent diffusely scattering spherical objects. As we do throughout our work, we typically assume an albedo of 0.12 unless stated otherwise.

These data were provided to JTMA in order to test the feasibility of faint streak detection in imagery such as this. We were able to bring to bear some new techniques to hunt for short, low signal-to-noise streaks. For a data set such as this, where immediate follow-up is not the goal – these images were over 4 years old – far more sensitive methods can be used that would not be practical computationally in a real-time system for a small telescope (though not necessarily when compared to the cost of a 6.5m telescope). This preliminary analysis shows the potential for streak finding in existing data sets. Figures 8, 9 and 10 show two of the three objects detected, one of which was very bright and thus not truly testing our techniques. The other two appear to be slightly sub-GEO at a few degrees inclination.

Figure 8 shows the brighter of the faint detections, found in the first two of the 9 provided images and the first of which is shown in Figure 8. It was detected with a flux of 2370 photoelectrons at a significance of 11.9σ. This object moved approximately 34 pixels during the 5 second exposure time, which when added to the GEO rate because these are untracked exposures, gives an approximate net apparent rate of 16.4 "/s. This rate corresponds to a circular orbit roughly 2400 km below GEO at an inclination of 8.7˚. Figure 9 shows the extracted light curve of this object used to determine the endpoints. The comparison of the measured streak intensity to the photometric reference star observations is somewhat fraught, as photometric accuracy requires one to use large measurement apertures. The photometric standard is 100 times brighter and thus extends to a large number of pixels. Applying the same aperture to this detection leads to very large uncertainties because the signal-to-noise drops. As an interim compromise, we report here conservative upper limits on brightness and size for both this and the other confirmed object. For this first object, the upper limit is r-band magnitude > 20.0, which is roughly a 13 cm diameter diffuse reflector at the inferred circular orbit range.
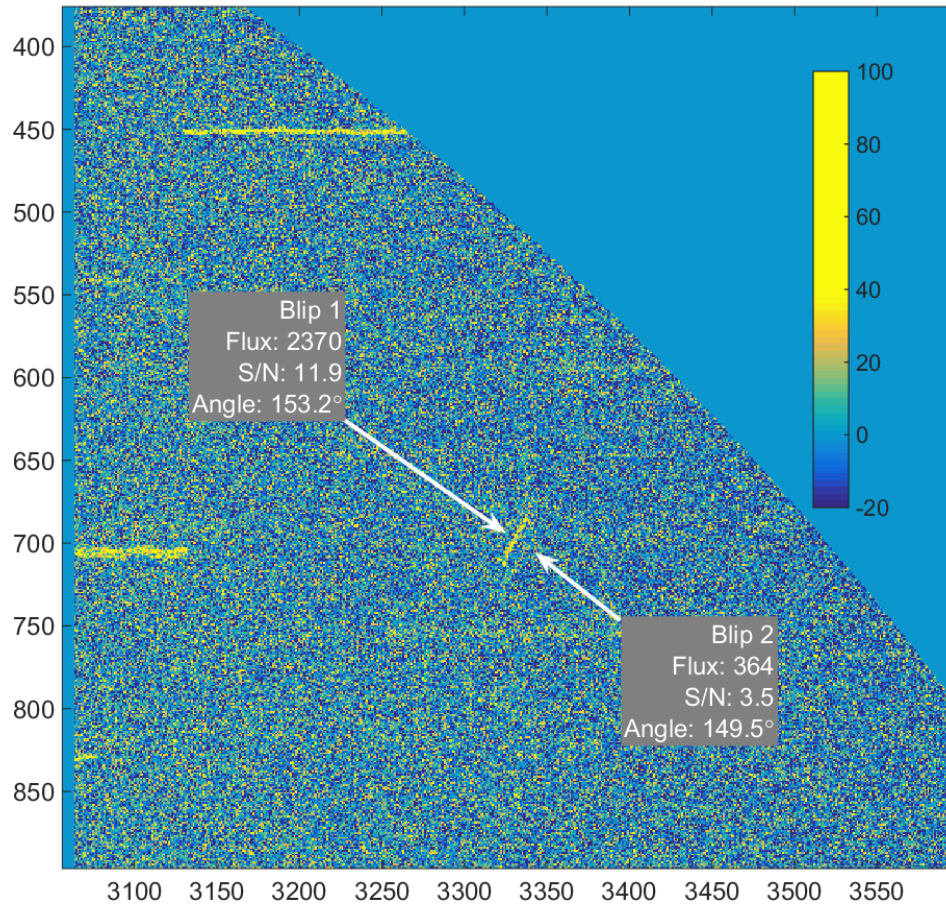
Figure 8 – This figure show the detection of an object in the first of the supplied Magellan images. Based on the provided photometric calibration, the object is fainter than r-band magnitude 20 and corresponds to an object smaller than 13cm diameter in a circular orbit 2400 km below GEO. The second object identified in this image was a 3.5σ detection at a suspiciously similar angle as the brighter object. However, the bright object persists in the next image, confirming it as a near GEO object, whereas this fainter object does not reappear. In images of this size, 3.5σ fluctuations are common and this one only arose suspicion because of proximity and similarity to the other object.
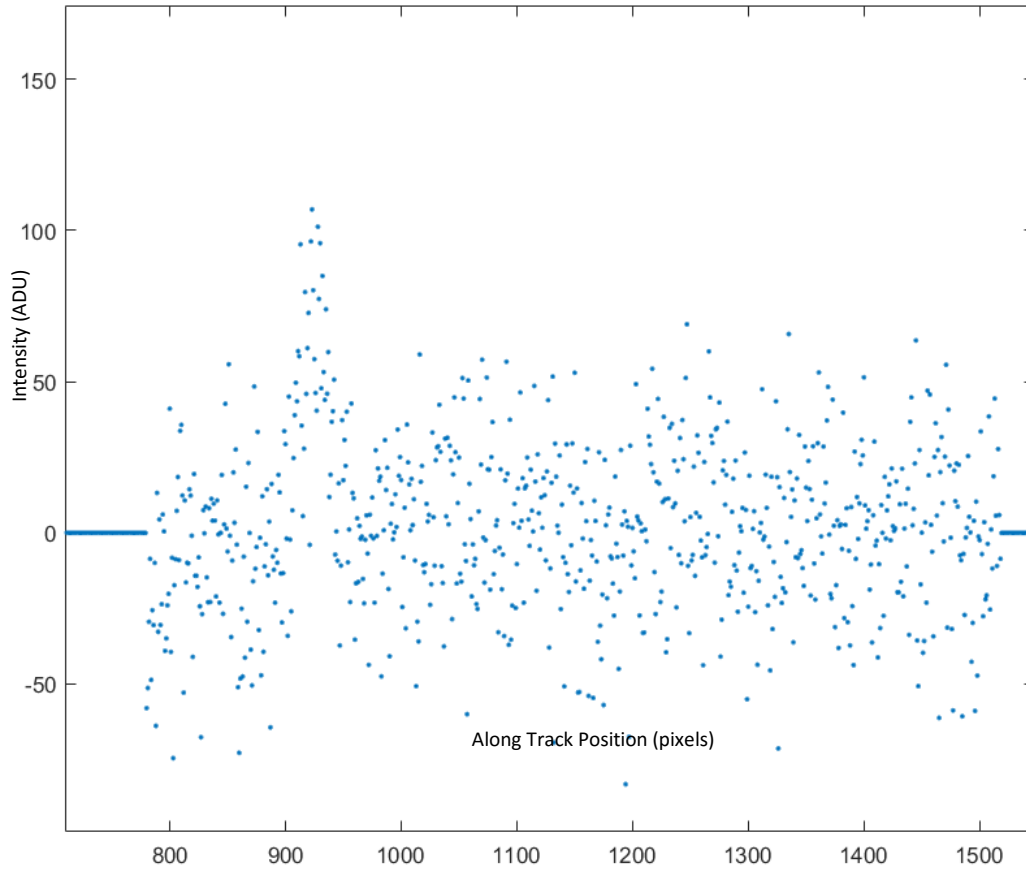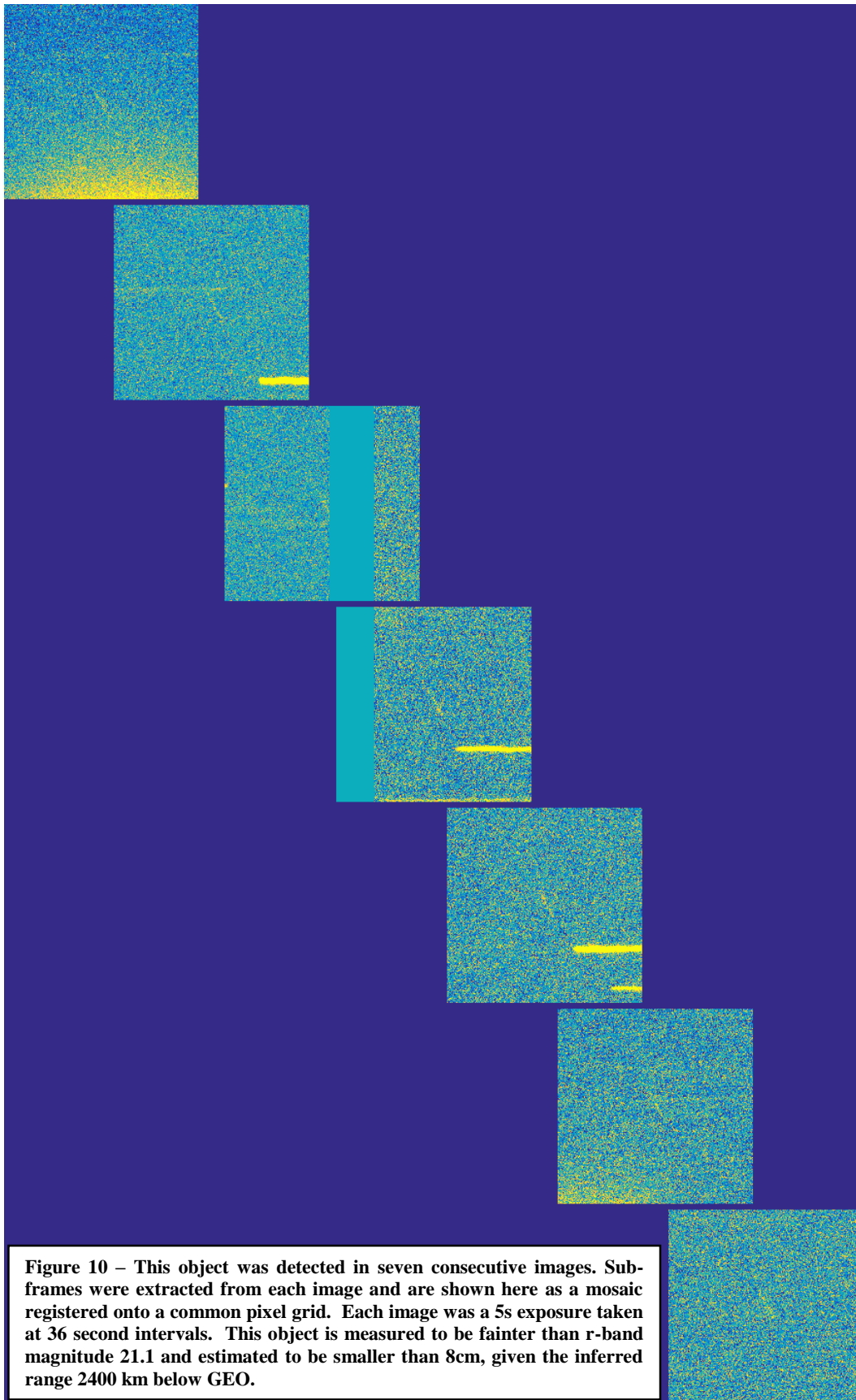
Figure 9 – Extracted light curve of the faint object in Figure 8.

A second possible object was detected near this first detection with nearly the same measured angle, though its significance was only 3.5σ. However, unlike the first object, it did not persist into the second image nor was it bright enough to assess rate or inclination to any useful degree. The first object moves out of the field of view immediately after the second image.

Figure 10 shows a sequence of sub-frames from images 3 through 9 registered to common pixel grid. The detected object is shown travelling from upper left to lower right though the field of view. The rate is suspiciously similar to the object in Figure 8 at 16.4 ”/s, but the inclination of this object's motion is -8.1° This object varies between 4σ and 5σ significance in our detection process, with an average signal of 750 e-. The lower significance would not normally be considered when used in our real-time detection scheme, but for this configuration and small image set, we were able to consider less significant potential objects. There were a number of other possible detections at this significance level, but none persisted into other images and so were not considered further. The object flux corresponds to an r-band magnitude greater than 21.1 and a size smaller than 8 cm at the inferred range.

Figure 10 – This object was detected in seven consecutive images. Sub-frames were extracted from each image and are shown here as a mosaic registered onto a common pixel grid. Each image was a 5s exposure taken at 36 second intervals. This object is measured to be fainter than r-band magnitude 21.1 and estimated to be smaller than 8cm, given the inferred range 2400 km below GEO.

7. Conclusions

JTMA continues to develop techniques for wide-field, real time ground-based optical surveillance of space and the detection of faint moving objects in astronomical imagery. We've demonstrated the capability of detecting small objects in Earth orbit in LEO and MEO using small, passive optical telescopes. These techniques rely on optimizing the tightly coupled parameters of optical design, detector matching, survey design and software, wherein the latter requires GPU-based acceleration to be able to process images quickly and generate orbit estimates for follow-up observations. By continuing to build new telescopes and new techniques, we are driving the cost of ground-based optical space surveillance down to a level where, in spite of its operational shortcomings with respect to weather and illumination conditions, the net gain in capability will be very much cost effective and significant – a national or global network of dozens of small telescopes would be very effective at a small fraction of the cost of a large radar installation or large optical telescope.

REFERENCES

[1] Bruck, Robert F., Copley, Robert H. "GEODSS Present Configuration and Potential" *Proceedings of the 2014 AMOS Technical Conference*, 2014.

[2] Zimmer, Peter C., McGraw, John T., Ackermann, Mark R., "Demonstration of Uncued Surveillance of LEO *"*, *Proceedings of the 2014 AMOS Technical Conference*, 2014.

[3] Zimmer, Peter C., Ackermann, Mark R., McGraw, John T. "GPU Accelerated Faint Streak Detection for Uncued Surveillance of LEO*"*, *Proceedings of the 2013 AMOS Technical Conference*, 2013.

[4] Ackermann, Mark R., Kiziah, Rex R., Zimmer, Peter C., Beason, J. Douglas, Spillar, Earl J., Cox, David D., McGraw, John T., Vestrand, W. Thomas "Affordable Options for Ground-based, Large-aperture Optical Space Surveillance Systems," *Proceedings of the 2013 AMOS Technical Conference*, 2013.

[5] Zimmer, Peter C., McGraw, John T., Ackermann, Mark R., "GPU-based Uncued Surveillance from LEO to GEO with Small Optical Telescopes," *Proceedings of 2015 AAS/AIAA Astrodynamics Specialist Conference*, 2015.

[6] Earl, Michael A., "Determining the Orbital Height of a Low-Earth-Orbiting Artificial Satellite Observed near the Local Zenith," *Journal of the Royal Astronomical Society of Canada* 100, 199 (2006).

[7] The United States government agency responsible for space situational awareness (SSA) information, U.S. Strategic Command (USSTRATCOM), provides online access to a catalog of tracked space objects at https://www.space-track.org/

[8] Weber, R. R., Alexander J. K., and R. G. Stone, "The Radio Astronomy Explorer Satellite, a Low-Frequency Observatory" *Radio Sci.,* v. 6, p. 1085, 1971.

[9] Lyndon B. Johnson Space Center Report. "Haystack and HAX Radar Measurements of the Orbital Debris Environment; 2003." (2006).

[10] Ackermann, Mark R., McGraw, John T., Martin, Jeffrey B., Zimmer, Peter C. 2003, "Blind Search for Micro Satellites in LEO: Optical Signatures and Search Strategies", *Proceedings of the 2003 AMOS Technical Conference*, also published as Report No.: SAND2003-3225C, Sandia National Laboratories, Albuquerque, NM (USA), September 2003.

[11] Seitzer, P., *et al*., "A Search for Optically Faint GEO Debris," *Proceedings of the 2011 AMOS Technical Conference*, 2011.

[12] Seitzer, P. *et al*., in preparation.